ACS Sustainable Chemistry & Engineering

pubs.acs.org/journal/ascecg

Letter

Multifunctional Catalysts for Direct Conversion of Alcohols to Long-Chain Hydrocarbons via Deoxygenative Olefination

Diana Ainembabazi, Jonathan Horlyck, Darren Dolan, Matthew Finn, Adam Fraser Lee, Karen Wilson, and Adelina Voutchkova-Kostal*

Cite This: *ACS Sustainable Chem. Eng.* 2021, 9, 14657−14662

Read Online

ACCESS | Metrics & More | Article Recommendations | Supporting Information

ABSTRACT: Multistep H_2-free upgrading of alcohols to liquid hydrocarbons is highly desirable for producing drop-in fuel substitutes, but the limited reports of this process for select substrates require multiple catalysts and bases, resulting in limited applicability. Direct conversion processes that rely on multifunctional catalysts and do not require base are yet to be reported. Here we describe such a Pd-catalyzed deoxygenative coupling of heptanol with heterogeneous catalysts composed of Pd immobilized on acid−base supports, which actively participate in the reaction cascade. The supports include primarily basic MgO, acidic γ-Al_2O_3, and Mg−Al hydrotalcite (HT), with a combination of Lewis acidic and basic sites. Pd−HTs with 1% and 5 wt % Pd loading afforded the highest overall activity in the multistep cascade, yielding 30% hydrocarbons (tridecene 6-*E*-tridecene and tridecane) from a neat reaction with heptanol with 0.2 mol % Pd loading. Heterogeneity tests suggest that Pd−HT is operationally heterogeneous. The impact of support selection on the activity and selectivity offers insights into the design principles for next-generation catalysts for this process and related transformations.

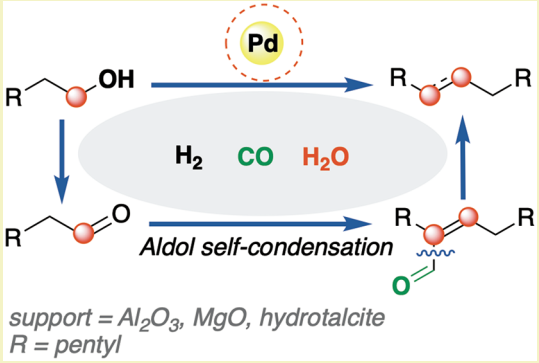

KEYWORDS: *Fuels from renewable alcohols, Decarbonylation, Olefination, Dehydrogenation, Palladium, Alumina, Magnesium oxide, Hydrotalcite*

INTRODUCTION

The ability to produce hydrocarbon fuels from renewable alcohols is an attractive strategy for producing drop-in substitutes for energy-dense fuels[1] and platform chemicals for petrochemical processes. Renewable alcohols are becoming increasingly abundant,[2] surpassing 100 million metric tons globally for C2−C4 alcohols alone,[3] and increasingly cost-competitive with fossil-fuel alternatives ($0.13−$0.16/L). Thus, there is intense interest in their efficient catalytic conversion to energy-dense hydrocarbons.[4] Practical processes for such transformations should be energy-efficient, use low-cost, robust, heterogeneous catalysts, and be tolerant to alcohol feedstreams of different concentrations. As highlighted in a recent life-cycle analysis of ethanol conversion processes, reducing the impact of such processes requires consolidation of multistep processes in a one-pot reaction to minimize reactor complexity, cost, and waste.[5] The latter necessitates the design of active and selective supported catalysts tailored for the tandem processes required to upgrade biomass-derived alcohols. Current approaches to upgrading alcohols primarily rely on Guerbet condensation, which affords longer-chain, branched primary alcohols through sequential dehydrogenation, aldol condensation, and hydrogenation reactions (Scheme 1, Reaction *A*).[6−17] The latter can be catalyzed by supported noble metal catalysts, metal oxides, and mixed metal oxides (MMOs).[6,7,11−13,16−18]

Scheme 1. Upgrading of Primary Alcohols to Longer Chain Alcohols (a) and Hydrocarbons (b)

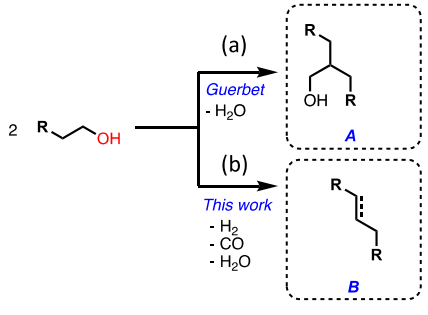

Received: August 10, 2021
Revised: October 19, 2021
Published: October 26, 2021

Scheme 2. Proposed Mechanism for Deoxygenative Olefination of Alcohols to Hydrocarbons and Other Byproducts

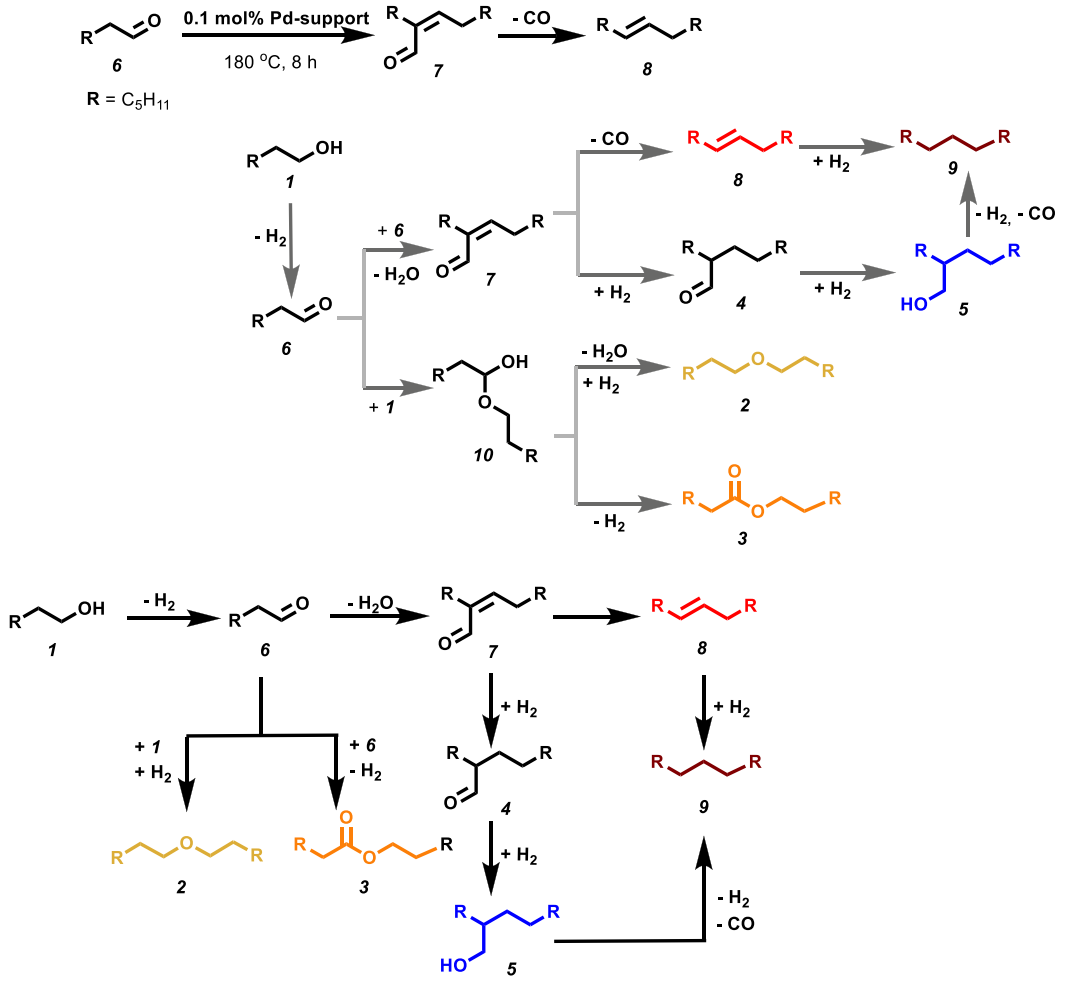

While the Guerbet reaction partially deoxygenates alcohols, complete alcohol deoxygenation via deoxygenative olefination (Scheme 1, Reaction *B*) has only been achieved for 2-aryl ethanol derivatives. Specifically, homogeneous Ir,[19] Ru,[20] and Mn[21] catalysts and a Ru heterogeneous catalyst[22] have been shown to facilitate dehydrogenation of 2-aryl ethanols, followed by base-promoted aldol condensation and decarbonylation. While the sequence is very atom-economical, the base-promoted decarbonylation limits the substrate scope[19] and results in high E-factors (3.9−38.1, Supporting Information (SI) Table S1). Deoxygenative olefination, to the best of our knowledge, has not been demonstrated for (i) aliphatic alcohols, (ii) in the absence of base, and (iii) using a single heterogeneous catalyst. However, Pd-catalyzed deoxygenative amination of biomass-derived phenols has been reported, affording biaryl amines.[23] Effecting the tandem transformations in a one-pot reaction necessitates multifunctional catalysts possessing catalytic sites effective for dehydrogenation, aldol condensation, and decarbonylation. Optimizing the formulation and operation of multifunctional catalysts is generally challenging, since it hinges on controlling the activity and selectivity of several interdependent steps. The latter requires control over the size, location, and structure of catalytically active species, and mechanistic insight into corresponding structure−activity relationships, including the role of supports.[24] Efforts by our group and others to develop Pd catalysts on active, tunable supports for organic synthesis and biomass valorization take advantage of cooperative catalytic activity of the support and strong interactions with support matrices that regulate metal speciation, reactivity, and stability.[25−32]

MgO and γ-Al_2O_3 supported metal catalysts are well-known to present divergent acid−base properties:[33−36] Saad et al. reported that Pt-supported MgO displays strong basicity, whereas Pt−Al_2O_3 displays strong acidity.[32] Similar observations were made by Groppo et al. for Pd analogues.[37] Hydrotalcites (HTs) are a subset of layered double hydroxides (LDHs) with the formula $[M_{1-x}^{2+}M_x^{3+}(OH)_2]^{x+}(A^{n-})_{x/n}\cdot mH_2O$, where M^{2+} and M^{3+} are Mg^2, Al^{3+}, or compatible alkali earth and transition metal cations.[38] Although LDH materials, similar to HTs, exhibit basic properties approaching those of MgO,[39] the tunable nature of such materials means that both O^{2-} Lewis base and Al^{3+} Lewis acid centers are accessible.[40,41]

The unique reactivity of Pd-doped LDH (or HT) catalysts includes decarbonylation of aldehydes,[27] aldol condensations,[25] and acceptorless alcohol and amine dehydrogenation:[26,42] elementary steps in deoxygenative olefination of alcohols. Recently, we reported that Pd−HT catalysts are highly active for the atom-economical olefination of carbonyls via aldol-decarbonylative coupling, producing only CO and H_2O byproducts.[25] We postulated that similar catalysts could be applied to alcohols to selectively form long-chain hydro-

https://doi.org/10.1021/acssuschemeng.1c05436
ACS Sustainable Chem. Eng. 2021, 9, 14657−14662

carbons via initial acceptorless dehydrogenation of the alcohol. The significantly higher barrier for decarbonylation than aldol condensation was expected to control the reaction sequence, such that initial alcohol dehydrogenation would afford the aldehyde, which would then undergo stepwise aldol condensation and decarbonylation to the alkene (Scheme 2).

Here we demonstrate the feasibility of one-pot, hydrogen-free, and base-free alcohol upgrading and deoxygenation over multifunctional Pd catalysts, featuring supports possessing different acid–base properties:[43,44] MgO, with primarily basic character; a hydrotalcite (HT) support with Lewis acidic and basic sites; and γ-Al_2O_3, with primarily acidic character. In this initial report we focus on heptanol as a substrate, but this process can be readily adapted to other aliphatic alcohols.

RESULTS AND DISCUSSION

Catalyst Synthesis and Characterization. Pd–γ-Al_2O_3 was synthesized by wet impregnation using commercial γ-Al_2O_3, while Pd–MgO and Pd–HT were synthesized via continuous coprecipitation previously described by us for HTs[45] and Pd–HTs.[27] Pd loading was targeted at 1–2 wt %. Pd–HT with higher loading (5 wt %) was also prepared to examine the effect of Pd loading. Physicochemical properties and Pd composition were investigated by ICP-AES, BET, TEM, XPS, and powder XRD (see catalyst characterization in Table S2). Powder XRD of Pd–γ-Al_2O_3 and Pd–HTs only show reflections for the respective supports, indicating that Pd is highly dispersed (Figure S2). The diffractogram of Pd–MgO, however, shows reflections associated with crystalline PdO phases, in addition to reflections characteristic of brucite nanocrystals. Crystallographic parameters of Pd–HTs are consistent with those of the unmodified support (Table S3). Catalyst acidity and basicity were determined by studying NH_3 and CO_2 temperature-programmed desorption (TPD) (Figure S4). In line with prior reports,[46,47] TPD spectra reveal that Pd–MgO has a high number of base sites of weak–moderate strength (CO_2 desorption spanning 50–400 °C), whereas Pd–Al_2O_3 has abundant weak–strong acid sites (NH_3 desorption spanning 50–500 °C). Both Pd–HTs exhibit significant acid–basic character and possess more moderate-strength basic sites than Pd–MgO, irrespective of Pd loading, indicating that support selection is the primary factor in determining the overall catalyst acid–base character. XPS revealed some differences in Pd surface speciation for the four catalysts (Figure S2). All catalysts comprise Pd^{2+} as the major species in addition to Pd^0, with Pd–MgO, Pd–Al_2O_3, and Pd–HT also exhibiting a low level of Pd^{4+}. The Pd^{2+} surface concentration was highest for Pd–Al_2O_3 (87%), whereas 5% Pd–HT shows the greatest Pd^0 concentration (42%), suggesting that the support acid–base properties impact Pd speciation.[27] Corresponding TEM images (Figure 1) reveal oxide agglomerates decorated with palladium nanoparticles typical of wet impregnation syntheses.[48,49] Nanoparticles (NPs) dispersed over Al_2O_3 and HT supports exhibited size and shape uniformity, with mean diameters of 3.7, 1.5, and 2.4 nm respectively for Pd–Al_2O_3, Pd–HT, and 5% Pd–HT. HRTEM of Pd–HT and Pd–Al_2O_3 shows only Pd(111), while 5% Pd–HT shows Pd(111) and PdO(110) phases (Figure S3). No lattice fringes were observable by TEM for Pd–MgO, and hence, the nature of the corresponding Pd phase could not be directly assigned; however, XRD identified reflections consistent with PdO(101), (112), and (220) planes.

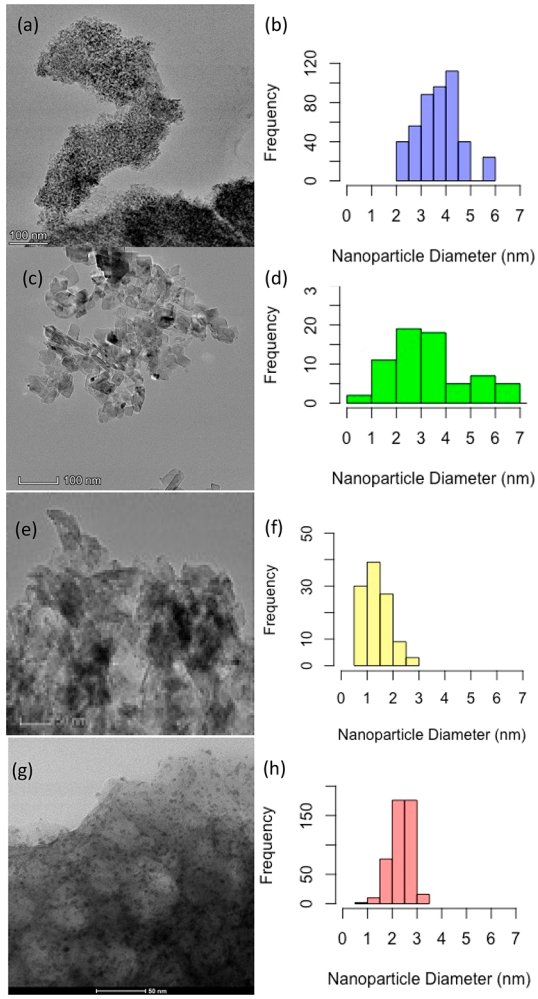

Figure 1. Bright-field TEM images and corresponding Pd particle size distributions for (a,b) Pd–Al_2O_3, (c,d) Pd–MgO, (e,f) Pd–HT, and (g,h) 5% Pd–HT.

Catalytic Activity for Deoxygenative Coupling. The Pd catalysts were subsequently tested for alcohol coupling using heptanol (***1***) as the substrate at 180 °C, based on previously optimized conditions for aldol-decarbonylation.[25] The proposed mechanism for the process is shown in Scheme 2. Initial dehydrogenation produces aldehyde ***6***, which can either undergo ketal hydrogenolysis[50] to form ***2***, alcohol coupling and dehydrogenation to form ester ***3***, or aldol condensation to form ***7***. Double transfer hydrogenation (TH) of ***7*** (with hydrogen adatoms from alcohol dehydrogenation) forms the Guerbet alcohol ***5***; alternatively, decarbonylation of ***7*** forms alkene ***8***, which can be hydrogenated to alkane ***9*** over Pd metal. As reported by Li et al.[15] and Zhang et al.,[10] the selectivity for ***5*** is promoted by co-operative acid and base catalysis, as possible for Pd–HT. It is also possible for ***5*** to undergo dehydrogenation and decarbonylation to form ***9***.

Control reactions with Pd-free MgO, HT and γ-Al_2O_3 supports showed no heptanol conversion. Pd–Al_2O_3 afforded >90% alcohol conversion in 48 h, with diheptyl ether as the major product (***2***, 97% selectivity, Table S4). Only trace heptyl heptanoate (***3***) and no alkene or alkane products were observed (Figure 2). This high ether selectivity is attributed to Pd-catalyzed hydrogenolysis of ketal ***10***, for which there is precedent using supported Pd catalysts.[41] Given that γ-Al_2O_3

https://doi.org/10.1021/acssuschemeng.1c05436
ACS Sustainable Chem. Eng. 2021, 9, 14657–14662

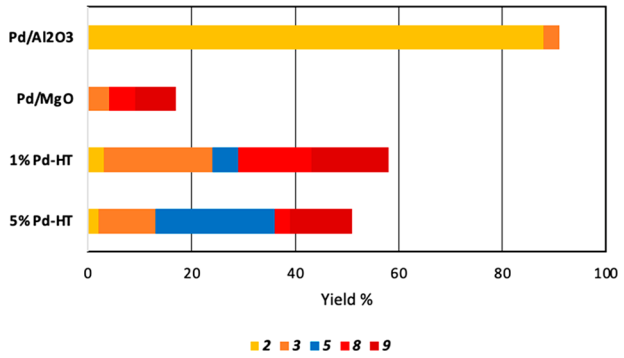

Figure 2. Product yield and selectivity for deoxygenative olefination of *n*-heptanol over supported Pd catalysts. See Scheme 2 for product structures. Conditions: 0.2 mol % Pd-support, 180 °C, 48 h.

affords no conversion with either heptanol, or heptanal and heptanol, Pd is clearly required, which implicates the ketal hydrogenolysis route depicted in Scheme 2.

A comparable reaction with Pd−HT affords a negligible quantity of the ether (**2**). Instead, we observe near complete selectivity for products arising from aldol condensate **7** (Scheme 2): namely, 25% and 27% selectivity respectively for 6-*E*-tridecene (***8***) and tridecane (***9***), 9% for the Guerbet alcohol (**5**), and 62% ester **3** (with 58% alcohol conversion).

Compared to the other catalysts, Pd−MgO afforded significantly lower heptanol conversion (17%) but exhibited the highest selectivity for hydrocarbons ***8*** (29%) and ***9*** (47%), alongside ester **3**. These observations suggest that Pd−MgO possesses few or weak Lewis acidic sites and limited Pd metal sites, accounting for slower dehydrogenation. These features also favor decarbonylation over rehydrogenation of the aldol condensate **7**. Attempts to increase activity by increasing catalyst loading to 1 mol % did not afford higher hydrocarbon yields, but further reaction optimization can be explored.

While the Pd loading for the reactions was constant at 0.2 mol %, the Pd loading on the support had some variation (1−2 wt %, as did the Pd particle size distribution (Figure 1). To probe whether the observed reactivity differences are due to the support, rather than Pd loading on the support, we synthesized a 5% Pd−HT. The latter has slightly larger particle size (Figure 2) but affords comparable alcohol conversion to Pd−HT (1 wt % Pd) (52% vs 51%) albeit with slightly lower selectivity of ***8*** and ***9*** (31% total yield vs 52% for Pd−HT). The 5% Pd−HT is also more selective for the Guerbet alcohol **5** over the ester **3** (Table S4), but this is attributed to the difference in total catalyst mass used in the reactions when controlling Pd loading: the larger mass of HT in the 1 wt % Pd−HT introduces additional water in the matrix, which may disfavor aldol condensation. In support of this theory, we showed that adding 20 μL of water to the reaction increases the selectivity for ester **3** over alcohol **5** by ∼10%. Thus, we conclude that the differences observed among the three catalysts arise from unique metal−support interactions and not differences in Pd surface loading or particle size.

In kinetic terms, the selectivity differences are driven by the relative rates of reactions of heptanal: fast aldol condensation favored by a high density of Brønsted basic sites increases selectivity for saturated oxygenates ***4*** and **5**, or alkenes/alkanes ***8***/***9***, while slower aldol gives way to formation of ketal ***10*** and its byproducts **2** and **3**. We thus expect supports with strongly basic sites to favor downstream aldol products, while those with stronger Lewis acidic sites to favor products from ketal ***10***. Consistent with this hypothesis, the catalyst on the most basic support, Pd−MgO, affords the highest selectivity for aldol products, while that on the most acidic support examined (Pd−Al_2O_3) affords almost exclusively products from ketal ***10***. Pd−HT, which is predominantly a basic support, also provides high selectivity for aldol condensate **7**. However, selectivity among aldol products depends on the relative rates of transfer hydrogenation versus decarbonylation of **7**. High selectivity to hydrocarbons requires faster decarbonylation, which is dependent on the Pd speciation.[27,51] To show that the reaction is not specific to heptanol, 1% Pd−HT was also tested with hexanol. Under closed vessel conditions the reaction affords comparable conversion and product distribution to that obtained for heptanol.

We briefly probed the gases evolved in reactions performed in a sealed vial at 180 °C. The hydrogen pop test was consistent with the presence of hydrogen. Under air, we identify CO_2 rather than CO by mass spectrometry. This is not surprising given that supported Pd catalysts are widely reported for CO oxidation; for example Ladas et al. observed high CO oxidation activity over dispersed Pd nanoparticles on Al_2O_3.[52]

Additional insights into catalyst design for this multistep process were sought from activity trends for the three steps: dehydrogenation, aldol condensation, and decarbonylation. Dehydrogenation was assessed from the total conversion, given that all products are derived from dehydrogenation, including ether **3** in the case of Pd−Al_2O_3. Thus, the trend follows Pd−Al_2O_3 > Pd−HT ∼ 5% Pd−HT > Pd−MgO. Activity for aldol condensation was assessed from reactions with heptanal at 100 °C, where no decarbonylation occurs. Based on the net 2 h yields of aldol condensate **7** (see Figure S5), the trend for aldol condensation follows Pd−MgO ∼ Pd−HT ≫ Pd−Al_2O_3, indicating that the strong basic sites on MgO and HT are significantly more effective for aldol condensation than the Lewis acidic sites of Al_2O_3. Trends in decarbonylation activity were assessed from 24 h reactions with heptanal at 150 °C based on percent of aldol product decarbonylated (Figure S6 for details). Under these conditions, the decarbonylation trend follows Pd−Al_2O_3 > Pd−HT > Pd−MgO. Comparing this trend to the lower selectivity observed for hydrocarbons ***8*** and ***9*** using 5% Pd−HT vs Pd−MgO (Pd−HT affords ∼3:2 ratio of Guerbet alcohol (**5**) to ***8*** and ***9*** vs Pd−MgO affords no alcohol **5**), we conclude that it is not that 5% Pd−HT is a less efficient decarbonylation catalyst than Pd−MgO, but rather that it facilitates competing transfer hydrogenation of **7**. The relative competence of the catalysts for the three steps (Figure 3) suggests that obtaining high activity and selectivity for hydrocarbons requires a balanced efficiency for each of the three steps and limiting competing ketal hydrogenolysis and transfer hydrogenation.

To rationalize the ratio of alkene ***8*** versus alkane ***9***, and thus, the ability of the catalyst to facilitate transfer hydrogenation of alkenes, we compared the catalyst efficiency for the TH of 6-*E*-tridecene (***8*** in Scheme 2) using 2-propanol as an efficient hydrogen donor (Scheme 3). Pd−MgO afforded ∼4-fold lower yield of alkane than Pd−HT (18% vs 62%), consistent with the lower fraction of ***9***:***8*** afforded by Pd−MgO in the heptanol reaction (1:1.7 for and 1:4 with Pd−MgO and Pd−HT respectively, Figure 2). This trend is also consistent with the higher heptanol conversion observed with Pd−HT compared to Pd−MgO. Interestingly, Pd−Al_2O_3 affords 51% yield of ***9***

https://doi.org/10.1021/acssuschemeng.1c05436
ACS Sustainable Chem. Eng. 2021, 9, 14657−14662

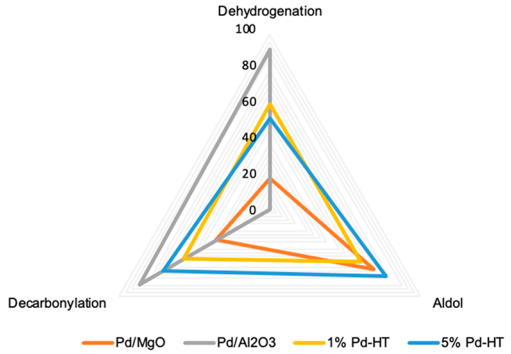

Figure 3. Radial plot of catalytic activity for the three-step deoxygenative olefination of alcohols. Data described in Table S5.

Scheme 3. Transfer Hydrogenation of Tridec-6-ene (*8*) Using 2-Propanol

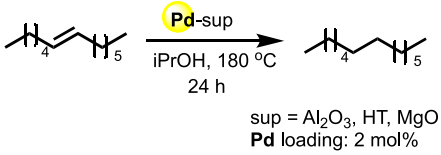

from *8*, suggesting it too is an efficient TH catalyst, although its high selectivity for ether *2* makes it insignificant for this reaction. In a similar experiment with aldol product *7*, we find Pd−HT is ∼2-fold more active than Pd−MgO for formation of alcohol *5*. Thus, the selectivity of Pd−MgO for *8* and *9* over *5* is the result of its faster decarbonylation and slower TH relative to that of Pd−HT.

While we intend to investigate the stability of these catalysts under continuous flow conditions in a full report, elemental analysis of the postreaction of the 5% Pd−HT shows a small loss of Pd and Mg (<10%, Table S4). HRTEM images of this used catalyst do not indicate extensive morphological changes but do show a small increase in mean particle size, from 2.4 to 3.4 nm nanoparticles (Figure S7) and a broadening of the particle size distribution. HRTEM also identified two Pd phases: reduced Pd(111) and PdO(101). Powder XRD of the used Pd−HT does not show reflections of Pd phases. We briefly examined whether decarbonylation was driven by soluble Pd species using poisoning tests with 1,10-phenanthroline as a scavenger of soluble Pd.[53] Addition of 5 equiv of 1,10-phenanthroline relative to total Pd only resulted in a 22% reduction of activity, suggesting catalysis is predominantly heterogeneous. A hot filtration test was also performed by sampling a portion of the reaction mixture after 3 h and passing this through a 2-μm hot frit. Product concentrations of the filtrate did not change significantly over the following 5 h, suggesting lack of catalytically competent soluble species. None of the metals could not be detected in solution postreaction by ICP-AES. These results are consistent with our previous findings for a decarbonylation catalyst[27] but are not definitive without planned operando studies to establish whether soluble Pd species play a significant role in any of the steps in the cascade.

CONCLUSION

Pd immobilized on basic supports at 1−2 wt % loading, such as MgO and hydrotalcite (HT), yields promising catalysts for an atom-economical alcohol upgrading to long-chain hydrocarbons, proceeding via tandem dehydrogenation, aldol condensation, and decarbonylation. Initial results with heptanol suggest that the support acid−base properties are the primary factors influencing catalyst activity and selectivity, likely due to their influence on the Pd speciation and ability to facilitate aldol condensation. Pd−MgO exhibits the highest selectivity to alkene and alkane products, but lowest conversion, whereas Pd−HT offers higher conversion albeit with slightly lower selectivity for hydrocarbons. Pd−Al_2O_3 affords only ether product due to faster ketal hydrogenolysis versus aldol condensation. Optimizing selectivity for deoxygenative coupling requires synergy between active Pd species and support basic sites, as well as optimization of the four sequential catalytic steps required for the overall transformation. Further mechanistic investigations that can inform the design of more active and selective multifunctional catalysts for this attractive alcohol coupling pathway are underway.

ASSOCIATED CONTENT

Supporting Information

The Supporting Information is available free of charge at https://pubs.acs.org/doi/10.1021/acssuschemeng.1c05436.

Details of catalyst synthesis, characterization, additional figures, and NMR characterization of products (PDF)

AUTHOR INFORMATION

Corresponding Author

Adelina Voutchkova-Kostal − *Chemistry Department, The George Washington University, Washington, D.C. 20052, United States;* orcid.org/0000-0002-7016-5244; Email: avoutchkova@gwu.edu

Authors

Diana Ainembabazi − *Chemistry Department, The George Washington University, Washington, D.C. 20052, United States*

Jonathan Horlyck − *Chemistry Department, The George Washington University, Washington, D.C. 20052, United States;* orcid.org/0000-0003-2417-9044

Darren Dolan − *Chemistry Department, The George Washington University, Washington, D.C. 20052, United States*

Matthew Finn − *Chemistry Department, The George Washington University, Washington, D.C. 20052, United States; Naval Research Laboratory, Washington, D.C. 20375, United States;* orcid.org/0000-0001-9474-7022

Adam Fraser Lee − *School of Science, RMIT University, Melbourne, VIC 3001, Australia;* orcid.org/0000-0002-2153-1391

Karen Wilson − *School of Science, RMIT University, Melbourne, VIC 3001, Australia;* orcid.org/0000-0003-4873-708X

Complete contact information is available at: https://pubs.acs.org/10.1021/acssuschemeng.1c05436

Funding

A.V.-K. thanks NSF CBET for support of this work (award 1805080); A.F.L. and K.W. acknowledge the ARC for support of this work (awards DPDP200100204 and DP200100313).

Notes

The authors declare no competing financial interest.

■ ACKNOWLEDGMENTS

In addition to funding sources listed above, we thank the GWU Material Institute and Surface Analysis Center at University of Maryland for use of instrumentation in catalyst characterization. We also thank the Naval Research Laboratory for use of gas adsorption analysis.

■ REFERENCES

(1) Huber, G. W.; Chheda, J. N.; Barrett, C. J.; Dumesic, J. A. *Science* **2005**, *308* (5727), 1446−1450.
(2) Sun, D.; Sato, S.; Ueda, W.; Primo, A.; Garcia, H.; Corma, A. *Green Chem.* **2016**, *18* (9), 2579−2597.
(3) US Energy Informationn Administration (E.I.A.). Monthly Energy Review, Table 10.3. https://www.eia.gov/totalenergy/data/monthly/#renewable (accessed Oct 2, 2021).
(4) Kuhz, H.; Kuenz, A.; Prüße, U.; Willke, T.; Vorlop, K.-D.; Wagemann, K.; Tippkötter, N. Products Components: Alcohols. *Biorefineries* **2017**, *166*, 339−372.
(5) Hannon, J. R.; Lynd, L. R.; Andrade, O.; Benavides, P. T.; Beckham, G. T.; Biddy, M. J.; Brown, N.; Chagas, M. F.; Davison, B. H.; Foust, T.; Junqueira, T. L.; Laser, M. S.; Li, Z. L.; Richard, T.; Tao, L.; Tuskan, G. A.; Wang, M. C.; Woods, J.; Wyman, C. E. *Proc. Natl. Acad. Sci. U. S. A.* **2020**, *117* (23), 12576−12583.
(6) Barrett, J. A.; Jones, Z. R.; Stickelmaier, C.; Schopp, N.; Ford, P. C. *ACS Sustainable Chem. Eng.* **2018**, *6* (11), 15119−15126.
(7) Bravo-Suárez, J. J.; Subramaniam, B.; Chaudhari, R. V. *Appl. Catal., A* **2013**, *455*, 234−246.
(8) Sun, Z.; Couto Vasconcelos, A.; Bottari, G.; Stuart, M. C. A.; Bonura, G.; Cannilla, C.; Frusteri, F.; Barta, K. *ACS Sustainable Chem. Eng.* **2017**, *5* (2), 1738−1746.
(9) León, M.; Díaz, E.; Ordóñez, S. *Catal. Today* **2011**, *164* (1), 436−442.
(10) Zhang, J.; Shi, K.; An, Z.; Zhu, Y.; Shu, X.; Song, H.; Xiang, X.; He, J. *Ind. Eng. Chem. Res.* **2020**, *59* (8), 3342−3350.
(11) Larina, O. V.; Valihura, K. V.; Kyriienko, P. I.; Vlasenko, N. V.; Balakin, D. Y.; Khalakhan, I.; Čendak, T.; Soloviev, S. O.; Orlyk, S. M. *Appl. Catal., A* **2019**, *588*, 117265.
(12) Rechi Siqueira, M.; Micali Perrone, O.; Metzker, G.; de Oliveira Lisboa, D. C.; Thoméo, J. C.; Boscolo, M. *Mol. Catal.* **2019**, *476*, 110516.
(13) Benito, P.; Vaccari, A.; Antonetti, C.; Licursi, D.; Schiarioli, N.; Rodriguez-Castellón, E.; Raspolli Galletti, A. M. *J. Cleaner Prod.* **2019**, *209*, 1614−1623.
(14) Marx, S.; Ndaba, B. *Biofuels* **2021**, *12*, 861.
(15) Li, X. N.; Peng, S. S.; Feng, L. N.; Lu, S. Q.; Ma, L. J.; Yue, M. B. *Microporous Mesoporous Mater.* **2018**, *261*, 44−50.
(16) León, M.; Díaz, E.; Vega, A.; Ordóñez, S.; Auroux, A. *Appl. Catal., B* **2011**, *102* (3), 590−599.
(17) Marcu, I.-C.; Tichit, D.; Fajula, F.; Tanchoux, N. *Catal. Today* **2009**, *147* (3), 231−238.
(18) Wang, J.; Yang, W.; Wu, C.; Gong, Y.; Zhang, J.; Shen, C. *ACS Sustainable Chem. Eng.* **2020**, *8* (45), 16960−16967.
(19) Obora, Y.; Anno, Y.; Okamoto, R.; Matsu-ura, T.; Ishii, Y. *Angew. Chem., Int. Ed.* **2011**, *50* (37), 8618−8622.
(20) Manojveer, S.; Forrest, S. J. K.; Johnson, M. T. *Chem. - Eur. J.* **2018**, *24* (4), 803−807.
(21) Wang, Y. J.; Shao, Z. H.; Zhang, K.; Liu, Q. *Angew. Chem., Int. Ed.* **2018**, *57* (46), 15143−15147.
(22) Cao, F.; Duan, Z. C.; Zhu, H. Y.; Wang, D. W. Deoxygenative coupling of 2-aryl-ethanols catalyzed by unsymmetrical pyrazolyl-pyridinyl-triazole ruthenium. *Mol. Catal.* **2021**, *503*, 111391.
(23) Li, J. S.; Qiu, Z. H.; Li, C. J. *Adv. Synth. Catal.* **2017**, *359* (20), 3648−3653.
(24) Crespo-Quesada, M.; Yarulin, A.; Jin, M. S.; Xia, Y. N.; Kiwi-Minsker, L. *J. Am. Chem. Soc.* **2011**, *133* (32), 12787−12794.
(25) Ainembabazi, D.; Reid, C.; Chen, A.; An, N.; Kostal, J.; Voutchkova-Kostal, A. *J. Am. Chem. Soc.* **2020**, *142* (2), 696−699.
(26) Ainembabazi, D.; An, N.; Manayil, J. C.; Wilson, K.; Lee, A. F.; Voutchkova-Kostal, A. M. *ACS Catal.* **2019**, *9* (2), 1055−1065.
(27) An, N.; Ainembabazi, D.; Reid, C.; Samudrala, K.; Wilson, K.; Lee, A. F.; Voutchkova-Kostal, A. *ChemSusChem* **2020**, *13* (2), 312−320.
(28) Stranick, M. A.; Houalla, M.; Hercules, D. M. *J. Catal.* **1990**, *125* (1), 214−226.
(29) Davantès, A.; Schlaup, C.; Carrier, X.; Rivallan, M.; Lefèvre, G. *J. Phys. Chem. C* **2017**, *121* (39), 21461−21471.
(30) Borg, O.; Dietzel, P.; Spjelkavik, A.; Tveten, E.; Walmsley, J.; Diplas, S.; Eri, S.; Holmen, A.; Rytter, E. *J. Catal.* **2008**, *259* (2), 161−164.
(31) Shelimov, B. N.; Lambert, J. F.; Che, M.; Didillon, B. *J. Mol. Catal. A: Chem.* **2000**, *158* (1), 91−99.
(32) Saad, F.; Comparot, J. D.; Brahmi, R.; Bensitel, M.; Pirault-Roy, L. *Appl. Catal., A* **2017**, *544*, 1−9.
(33) Xu, B.-Q.; Yamaguchi, T.; Tanabe, K. *Chem. Lett.* **1988**, *17* (10), 1663−1666.
(34) Aytam, H. P.; Akula, V.; Janmanchi, K.; Kamaraju, S. R. R.; Panja, K. R.; Gurram, K.; Niemantsverdriet, J. W. *J. Phys. Chem. B* **2002**, *106* (5), 1024−1031.
(35) Gac, W. *Appl. Surf. Sci.* **2011**, *257* (7), 2875−2880.
(36) Poupin, C.; Maache, R.; Pirault-Roy, L.; Brahmi, R.; Williams, C. T. *Appl. Catal., A* **2014**, *475*, 363−370.
(37) Groppo, E.; Bertarione, S.; Rotunno, F.; Agostini, G.; Scarano, D.; Pellegrini, R.; Leofanti, G.; Zecchina, A.; Lamberti, C. *J. Phys. Chem. C* **2007**, *111* (19), 7021−7028.
(38) Cavani, F.; Trifiro, F.; Vaccari, A. *Catal. Today* **1991**, *11* (2), 173−301.
(39) He, Y.; Yang, P.; Fan, J.; Liu, Y.; Du, Y.; Feng, J.; Fan, F.; Li, D. *RSC Adv.* **2015**, *5* (91), 74907−74915.
(40) Álvarez, M. G.; Chimentão, R. J.; Figueras, F.; Medina, F. *Appl. Clay Sci.* **2012**, *58*, 16−24.
(41) Pavel, O. D.; Tichit, D.; Marcu, I.-C. *Appl. Clay Sci.* **2012**, *61*, 52−58.
(42) Bain, J.; Cho, P.; Voutchkova-Kostal, A. *Green Chem.* **2015**, *17* (4), 2271−2280.
(43) Dawes, G. J. S.; Scott, E. L.; Le Nôtre, J.; Sanders, J. P. M.; Bitter, J. H. *Green Chem.* **2015**, *17* (6), 3231−3250.
(44) Lopez-Ruiz, J. A.; Davis, R. J. *Green Chem.* **2014**, *16* (2), 683−694.
(45) Yaseneva, P.; An, N.; Finn, M.; Tiedemann, N.; Jose, N.; Voutchkova-Kostal, A.; Lapkin, A. *Chem. Eng. J.* **2019**, *360*, 190−199.
(46) Saad, F.; Comparot, J. D.; Brahmi, R.; Bensitel, M.; Pirault-Roy, L. *Appl. Catal., A* **2017**, *544*, 1−9.
(47) Poupin, C.; Maache, R.; Pirault-Roy, L.; Brahmi, R.; Williams, C. T. *Appl. Catal., A* **2014**, *475*, 363−370.
(48) He, Y.; Fan, J.; Feng, J.; Luo, C.; Yang, P.; Li, D. *J. Catal.* **2015**, *331*, 118−127.
(49) Akuri, S. R.; Dhoke, C.; Rakesh, K.; Hegde, S.; Nair, S. A.; Deshpande, R.; Manikandan, P. *Catal. Lett.* **2017**, *147* (5), 1285−1293.
(50) Bethmont, V.; Montassier, C.; Marecot, P. *J. Mol. Catal. A: Chem.* **2000**, *152* (1−2), 133−140.
(51) Vorotnikov, V.; Mpourmpakis, G.; Vlachos, D. G. *ACS Catal.* **2012**, *2* (12), 2496−2504.
(52) Ladas, S.; Poppa, H.; Boudart, M. *Surf. Sci.* **1981**, *102* (1), 151−171.
(53) Bayram, E.; Finke, R. G. *ACS Catal.* **2012**, *2* (9), 1967−1975.

https://doi.org/10.1021/acssuschemeng.1c05436
ACS Sustainable Chem. Eng. 2021, 9, 14657−14662